FERMILAB-13-096-T

arXiv:1303.6178v1 [hep-ph] 25 Mar 2013

Correlated, Precision Measurements of θ_{23} and δ using only the Electron Neutrino Appearance Experiments

Hisakazu Minakata* and Stephen J. Parke†

Theoretical Physics Department,
Fermilab, P. O. Box 500,
Batavia, IL 60510, USA

(Dated: March 25, 2013)

Abstract

Precision measurement of the leptonic CP violating phase δ will suffer from the, then surviving, large uncertainty of $\sin^2\theta_{23}$ of $10-20\%$ in the experimentally interesting region near maximal mixing of θ_{23}. We advocate a new method for determination of both θ_{23} and δ at the same time using only the ν_e and $\bar{\nu}_e$ appearance channels, and show that $\sin^2\theta_{23}$ can be determined automatically with much higher accuracy, approximately a factor of six, than $\sin\delta$. In this method, we identify a new degeneracy for the simultaneous determination of θ_{23} and δ, the θ_{23} intrinsic degeneracy, which must be resolved in order to achieve precision measurement of these two parameters. Spectral information around the vacuum oscillation maxima is shown to be the best way to resolve this degeneracy.

PACS numbers: 14.60.Pq,14.60.Lm

*Electronic address: hisakazu.minakata@gmail.com
†Electronic address: parke@fnal.gov

Operated by Fermi Research Alliance, LLC under Contract No. De-AC02-07CH11359 with the United States Department of Energy.

I. INTRODUCTION

In neutrino oscillation physics, the traditional way of determining the leptonic CP violating phase, δ, is to measure δ together with θ_{13} by using ν_e and $\bar{\nu}_e$ appearance channels in muon neutrino superbeam experiments, (or similarly by ν_μ and $\bar{\nu}_\mu$ appearance in either neutrino factory or beta beam experiments). In posing the problem in this way, θ_{23} is assumed to be determined to high accuracy by a ν_μ disappearance measurement up to the octant degeneracy. But, now we need a new orientation to choose the right approach for the determination of δ, because:

- θ_{13} is already determined with high accuracy, and its precision will become even greater by the time δ is measured [1–5],
- and θ_{23} will be determined with less percentage accuracy than θ_{13} in the experimentally preferred region, see [6, 7], between 40° and 50°. Since the disappearance measurements will have difficulty in determining $s^2_{23} \equiv \sin^2\theta_{23}$ with an accuracy better than $10-20\%$ in this region [8].

How seriously does the uncertainty in s^2_{23} affect the sensitivity to δ? We show in Appendix A that the uncertainty of δ is approximately proportional to

$$\sqrt{(\Delta P/P)^2 + (\Delta\bar{P}/\bar{P})^2 + \eta(\Delta s^2_{23}/s^2_{23})^2} \tag{1}$$

where P and $\bar{P}$ are the ν_e and $\bar{\nu}_e$ appearance probabilities with uncertainties ΔP and $\Delta\bar{P}$, respectively, and Δs^2_{23} is the uncertainty on s^2_{23}, and η is generically a number of order unity. Thus, when the measurement enters into a precision era in which the percentage uncertainty on P and $\bar{P}$ would be smaller than, say 5%, the uncertainty of δ would be dominated by the s^2_{23} uncertainty[1].

In this paper, we present a new strategy for precision measurement of δ and θ_{23} to overcome this problem. Instead of using ν_μ disappearance channel for determination of θ_{23}, we rely on ν_e and $\bar{\nu}_e$ appearance measurement to determine precisely θ_{23} and δ at the same time. With this method the uncertainties expected for θ_{23} and δ are related with each other as follows

$$\Delta(s^2_{23}) \simeq \frac{1}{6}\Delta(\sin\delta), \tag{2}$$

near the first vacuum oscillation maximum, as shown in Sec. III B. Therefore, once we enter into the era in which $\sin\delta$ can be measured with reasonably high accuracy, s^2_{23} can be determined automatically with significantly higher accuracy than $\sin\delta$ which can be competitive with the disappearance measurement in the region $40° < \theta_{23} < 50°$. Of course, the disappearance measurement will provide supplemental information, and also serves as a consistency check on νSM.

This new setting, of simultaneous measurement of θ_{23} and δ, brings us to the problem of a new degeneracy involving these two parameters which we call the "θ_{23} intrinsic degeneracy" because of it's similarity to the θ_{13} intrinsic degeneracy [9]. Notice that this degeneracy is

[1] Note that this is a simplified discussion for the sake of clarity. A more detailed and accurate description can be found in Appendix A.

entirely different from the θ_{23} octant degeneracy discussed in [10]. We show that resolving this θ_{23} intrinsic degeneracy is crucial to achieve precision measurements of δ and θ_{23}, and that the disappearance measurement cannot help in region $\sin^2 2\theta_{23} \gtrsim 0.97$. We argue that spectrum information around the vacuum oscillation maximum peaks is the most powerful way to resolve the degeneracy. It may be possible that such spectrum analyses could be carried out with a narrow-band neutrino beam, but if it is not powerful enough, use of a wide-band beam could be required.

If the mass hierarchy is unknown the θ_{23} intrinsic degeneracy would be a part of a larger degeneracy similar to the conventional $\theta_{13} - \delta$ eightfold parameter degeneracy [9–11]. Here, we focus on the "intrinsic" part by simply assuming that the mass hierarchy will already be determined at the time when the precision measurement we discuss will be realized. The generalization to the case including the unknown mass hierarchy can be performed in a straightforward manner.

This paper is organized as follows: in Sec. II we introduce the θ_{23} intrinsic degeneracy, the stimultaneous measurements of δ and θ_{23} is discussed in detail in Sec. III & IV. In Sec. V & VI a simple toy analysis is given for a variety of possible future precision experiments. The conclusions are presented in Sec. VII. The three Appendices contain some mathematical derivations too detailed for the main body of the paper.

II. INTRODUCTION TO THE θ_{23} INTRINSIC DEGENERACY

We start by giving pedagogical reminder of the relevant issues, some of which have been discussed in the past, but not all of them. Suppose one could measure $\sin^2 2\theta_{23}$ to an uncertainty of 0.02 at, say, 95% C.L. Then, to what accuracy can one determine $\sin^2\theta_{23} \equiv s^2_{23}$? The answer to this question is given in the left panel in Fig. 1. In the region of θ_{23} far away from maximal, the loss of sensitivity to s^2_{23} is modest, apart from the octant issue, whereas for $\sin^2 2\theta_{23} \gtrsim 0.98$ the accuracy of s^2_{23} suddenly jumps to 10-20% level. This was observed in Fig. 3 of ref. [8] where they plotted the s^2_{23}-error as a function of $\sin^2 2\theta_{23}$.

In the left panel in Fig. 1, two vertical scales are provided for convenience of the readers. Observe that the nonlinearity of scales in mapping from s^2_{23} to $\sin^2 2\theta_{23}$ is large, and it is most significant in region where

$$\sin^2 2\theta_{23} \gtrsim 0.97 \quad \text{or} \quad 0.41 \leq \sin^2\theta_{23} \leq 0.59 \quad \text{or} \quad 40^\circ \leq \theta_{23} \leq 50^\circ. \tag{3}$$

This is the region with significant overlap with the experimentally preferred one [6, 7], and it is the region we are primarily interested in for the purposes of this paper.

In the right panel of Fig. 1, the bi-probability plot [11], gives the allowed values of $(P(\nu_\mu \to \nu_e),\ P(\bar{\nu}_\mu \to \bar{\nu}_e))$ for three set of values of $\sin^2 2\theta_{23}$ =0.9516, 0.9676 and 0.9996. Here, we have switched off the matter effect and restricted ourselves to the Normal Hierarchy. The figure shows that with an *exact* measurement of the ν_e and $\bar{\nu}_e$ appearance probabilities one can determine s^2_{23} and δ at the same time apart from the twofold degeneracy, which we call the θ_{23} intrinsic degeneracy. Notice that this degeneracy is completely different in nature from the θ_{23} octant degeneracy and exists for all values of θ_{23}, even at $\pi/4$.

To illuminate the nature of the new degeneracy on θ_{23} and δ, we place in the left panel of Fig. 1 three pairs of cross marks, distinguished also by color, corresponding to three sets of ellipse shown in the bi-probability plot, the right panel. In the two cases far off maximal mixing θ_{23} depicted by the blue and the red crosses, it is obvious that the degeneracy has

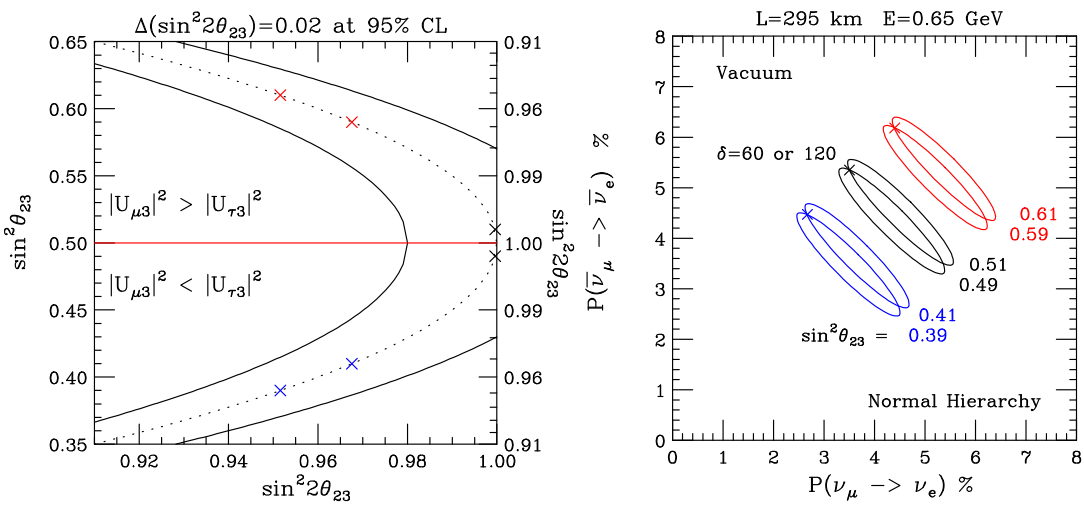

FIG. 1: Left panel: Allowed region in $\sin^2 2\theta_{23}$ vs. $\sin^2\theta_{23}$ space assuming 2% uncertainty of $\sin^2 2\theta_{23}$ by a ν_μ disappearance measurement. Right panel: The bi-probability plot in $P(\nu_\mu \to \nu_e)$ vs. $P(\bar{\nu}_\mu \to \bar{\nu}_e)$ space with three set of values of $P(\nu_\mu \to \nu_e)$ and $P(\bar{\nu}_\mu \to \bar{\nu}_e)$ which correspond to $\sin^2 2\theta_{23}$ approximately 0.96 (blue and red), 1.0 (black). The blue and red pair of ellipses are in different octants. The precise value of $\sin^2\theta_{23}$ of each ellipse is as indicated in the figure, and at the crossing points indicated by $\times$ the value of δ is 60° (120°) for larger (smaller) $\sin^2\theta_{23}$ ellipses, for the normal hierarchy. The colored crosses on the left panel correspond to the ellipse on the right panel.

nothing to do with the θ_{23} octant degeneracy. In the case near the maximal θ_{23} drawn by the black crosses in Fig. 1, the two solutions live in different octants, and we have a merging of the θ_{23} intrinsic degeneracy and the octant degeneracy for θ_{23} at very close to the maximal mixing.[2]

We note that the size of the ellipses does not change much with different values of θ_{23} because they scale as $\propto \sin 2\theta_{23}$ which changes very little near $\theta_{23} = \pi/4$. If the value of θ_{13} had been changed instead of θ_{23}, not only does the location of the bi-probability ellipse change but also its size changes with increasing or decreasing $\sin\theta_{13}$. Note also that in vacuum with arbitrary values of $\Delta \equiv \frac{\Delta m^2_{32} L}{4E}$, and in matter at vacuum oscillation maxima (VOM, $\Delta = \left(\frac{\pi}{2} + n\right)\pi$), the θ_{23} intrinsic degeneracy is a δ, $\pi - \delta$ degeneracy. It is because the difference between the degenerate solutions of $\sin\delta$ vanishes in vacuum (see (14)), and only $\sin\delta$ is determined at VOM. This is reminiscent of the θ_{13} intrinsic degeneracy first discussed in [9] but there are important differences. Understanding the nature of this degeneracy will be elaborated in the following three sections, III, IV, and V.

From the bi-probability plot given in Fig. 1, one can infer an interesting feature of the δ dependence of the error of δ. The uncertainty of θ_{23}, which allows the ellipses moving up and down, results in larger errors for δ determination at the both ends of the ellipses, i.e.,

[2] If the precise value of θ_{13} is known, adding only disappearance measurement produces the θ_{23} octant degeneracy. Adding only ν and $\bar{\nu}$ appearance measurement produces the θ_{23} intrinsic degeneracy, whose solutions may exist across the octant boundary for θ_{23} very close to maximal mixing (black line and crosses in Fig. 1). With a finite error of θ_{13}, the two degeneracies fuse in this region.

around $\delta \sim \pm\frac{\pi}{2}$, than at $\delta \sim 0$, or π. Therefore, the large uncertainty of s_{23}^2 described in (3) can produce broad peaks at $\delta \simeq \pm\frac{\pi}{2}$ in the δ dependence of δ error. In fact, this feature is seen in some of the figures (e.g., in Fig. 9) given in [12].

III. CORRELATED MEASUREMENTS OF θ_{23} AND δ BY ν_e AND $\bar{\nu}_e$ APPEARANCE CHANNELS

We demonstrate our new strategy by showing that simultaneous determination of θ_{23} and δ is the way to proceed. To illuminate the point we consider a counting experiment to measure the ν_e and $\bar{\nu}_e$ appearance probabilities at a given energy in matter;

$$\begin{aligned} P \equiv P(\nu_\mu \to \nu_e) &= 2s_{23}^2 A_\oplus^2 + 2\epsilon \sin 2\theta_{23} A_\oplus A_\odot \cos(\delta + \Delta) + 2c_{23}^2 \epsilon^2 A_\odot^2 \\ \bar{P} \equiv P(\bar{\nu}_\mu \to \bar{\nu}_e) &= 2s_{23}^2 \bar{A}_\oplus^2 + 2\epsilon \sin 2\theta_{23} \bar{A}_\oplus A_\odot \cos(\delta - \Delta) + 2c_{23}^2 \epsilon^2 A_\odot^2 \end{aligned} \tag{4}$$

where $\Delta \equiv \frac{\Delta m_{31}^2 L}{4E}$ and $\epsilon \equiv \frac{\Delta m_{21}^2}{\Delta m_{31}^2} \simeq 0.03$. The A functions in (4) are defined as

$$\begin{aligned} A_\oplus &\equiv \sqrt{2} s_{13} c_{13} \left(\frac{\Delta m_{31}^2}{\Delta m_{31}^2 - a}\right) \sin\left(\frac{(\Delta m_{31}^2 - a)L}{4E}\right) \\ \bar{A}_\oplus &\equiv \sqrt{2} s_{13} c_{13} \left(\frac{\Delta m_{31}^2}{\Delta m_{31}^2 + a}\right) \sin\left(\frac{(\Delta m_{31}^2 + a)L}{4E}\right) \\ A_\odot &\equiv \sqrt{2} c_{12} s_{12} c_{13} \left(\frac{\Delta m_{31}^2}{a}\right) \sin\left(\frac{aL}{4E}\right) = \bar{A}_\odot \end{aligned} \tag{5}$$

where

$$\begin{aligned} \frac{a}{\Delta m_{31}^2} &= \frac{2\sqrt{2} G_F N_e E_\nu}{\Delta m_{31}^2} \\ &= 8.5 \times 10^{-2} \left(\frac{\rho}{2.8 \text{ g/cm}^3}\right) \left(\frac{Y_e}{0.5}\right) \left(\frac{2.5 \times 10^{-3} \text{ eV}^2}{\Delta m_{31}^2}\right) \left(\frac{E}{1 \text{ GeV}}\right). \end{aligned} \tag{6}$$

$A_\odot$ is of order unity in most regions of relevant experimental parameters, but $A_\oplus$ and $\bar{A}_\oplus$ are suppressed by smallness of s_{13}. The A's are defined such that the atmospheric and the solar oscillation probabilities at the maximal mixing angle $\theta_{23} = \frac{\pi}{4}$, $P_\oplus$ and $P_\odot$ respectively, are given by $P_\oplus = A_\oplus^2$ and $P_\odot = \epsilon^2 A_\odot^2$. For simplicity we will ignore the $2c_{23}^2 \epsilon^2 A_\odot^2$ terms, in Eq. (4), in the rest of this paper as they are significantly smaller than the other terms.[3]

It is instructive to quote an estimation of the ratio of $A_\oplus$ to $\epsilon A_\odot$ in near vacuum environment, $\frac{a}{\Delta m_{31}^2} \ll 1$, assuming the experiment is performed near the first oscillation maximum, $\Delta \sim 1$,

$$\frac{A_\oplus}{\epsilon A_\odot} = \left(\frac{2s_{13}}{\sin 2\theta_{12}}\right) \frac{\sin\Delta}{\Delta} \left[1 + \frac{a}{\Delta m_{31}^2}(1 - \Delta \cot \Delta)\right] \left(\frac{\Delta m_{31}^2}{\Delta m_{21}^2}\right) \simeq 6. \tag{7}$$

As we will show later, the size of this ratio is significant for the relative size of the uncertainties for the measurement of $\sin^2\theta_{23}$ and δ.

[3] To include the effect of $2\epsilon^2 c_{23}^2 A_\odot^2$ terms, rewrite $c_{23}^2 = 1 - s_{23}^2$ and then the $2s_{23}^2 \epsilon^2 A_\odot^2$ can be included in the $A_\oplus^2$ terms and the $2\epsilon^2 A_\odot^2$ can be moved to the left hand side.

A. Measuring θ_{23} and δ at the first vacuum oscillation maximum

To show the point let us consider measurement at the first vacuum oscillation maximum (1st VOM), $\Delta = \frac{\pi}{2}$. Then, $\cos(\delta \pm \Delta) = \mp \sin\delta$. One can eliminate δ by combining the two equations in (4), then

$$(s_{23}^2)_0 \;=\; \frac{1}{2\left(A_\oplus + \bar{A}_\oplus\right)} \frac{1}{\sqrt{A_\oplus \bar{A}_\oplus}} \left[\bar{P} \left(\frac{A_\oplus}{\bar{A}_\oplus}\right)^{\frac{1}{2}} + P \left(\frac{\bar{A}_\oplus}{A_\oplus}\right)^{\frac{1}{2}} \right]. \tag{8}$$

If instead we eliminate the first terms of (4) in favor of $\sin\delta$ we obtain,

$$\sin\delta_0 \;=\; \frac{1}{2\sin 2\theta_{23}\left(A_\oplus + \bar{A}_\oplus\right)} \frac{1}{\epsilon A_\odot} \left[\bar{P} \left(\frac{A_\oplus}{\bar{A}_\oplus}\right) - P \left(\frac{\bar{A}_\oplus}{A_\oplus}\right) \right]. \tag{9}$$

$\cos\delta_0$ can be obtained as $\cos\delta_0 = \pm\sqrt{1-\sin^2\delta_0}$. Notice that the sign ambiguity $\delta \leftrightarrow \pi - \delta$ cannot be resolved by measurement here. Apart from the different linear combinations of P and $\bar{P}$, these two equations differ by the overall factors of $1/\sqrt{A_\oplus \bar{A}_\oplus}$ and $1/\epsilon A_\odot$ in s_{23}^2 and $\sin\delta$, respectively.

We use the matter perturbation theory to obtain a simpler expression which allows intuitive understanding. We assume $\frac{a}{\Delta m_{31}^2} \ll 1$, which is an excellent approximation for T2K, then we obtain, to first order in $\frac{a}{\Delta m_{31}^2}$,

$$\begin{aligned} (s_{23}^2)_0 \;&=\; \frac{1}{8 s_{13}^2} \left[\left(\bar{P} + P\right) + \frac{a}{\Delta m_{31}^2} \left(\bar{P} - P\right) \right], \\ \sin\delta_0 \;&=\; \frac{1}{8\epsilon J_r \pi} \left[(\bar{P} - P) + \frac{2a}{\Delta m_{31}^2} (\bar{P} + P) \right], \end{aligned} \tag{10}$$

where $J_r \equiv c_{12} s_{12} c_{23} s_{23} s_{13} c_{13}^2$. Therefore, at VOM and in near vacuum environment s_{23}^2 is determined by sum of the probabilities $\bar{P}+P$, while $\sin\delta$ is governed by the difference $\bar{P}-P$. $\bar{P}+P$ and $\bar{P}-P$ switch their positions to induce sub-leading corrections due to matter effect into s_{23}^2 and $\sin\delta$, as shown in (10).

B. Error of s_{23}^2 is smaller than that of $\sin\delta$

Let us estimate the expected errors in measurement of s_{23}^2 and $\sin\delta$, assuming that the errors for P and $\bar{P}$ are independent with each other. We also assume settings in which the matter effect remains subdominant and use notations $A_\oplus^{vac}$ for $A_\oplus = \bar{A}_\oplus$ in vacuum. Using (8) and (9), the errors, $\Delta(s_{23}^2)$ and $\Delta(\sin\delta)$, are given by

$$\begin{aligned} \Delta(s_{23}^2) \;&\approx\; \frac{1}{4(A_\oplus^{vac})^2} \sqrt{(\Delta P)^2 + (\Delta \bar{P})^2} \\ \Delta(\sin\delta) \;&\approx\; \frac{1}{4\sin 2\theta_{23} |A_\oplus^{vac}| (\epsilon A_\odot)} \sqrt{(\Delta P)^2 + (\Delta \bar{P})^2} \end{aligned} \tag{11}$$

Notice that the two errors are related with each other at the 1st VOM by

$$\Delta(s_{23}^2) \approx \left(\frac{\epsilon A_\odot}{|A_\oplus^{vac}|}\right) \Delta(\sin\delta) \simeq \frac{1}{6} \Delta(\sin\delta) \tag{12}$$

Therefore, once the experiment starts to measure $\sin\delta$, then s_{23}^2 can be determined with an uncertainty which is 6 times smaller. Thus, if a precision measurement of $\sin\delta$ is made, then the precision on s_{23}^2 becomes competitive with the precision from the disappearance measurement, and in fact far exceeds it at around the maximal mixing.

Notice that by using the appearance channels we are free from the θ_{23} octant degeneracy inherent in the disappearance channel. The expression of errors of s_{23}^2 and δ in more general setting, off VOM and in matter, is given in Appendix B.

If one estimates the s_{23}^2 error by using the simulation done by the Hyper-K collaboration [13], assuming 1.5 years of neutrino and 3.5 years of antineutrino runs with beam power of 1.65 MW, one finds find that the precision on s_{23}^2 exceeds the precision from the disappearance measurement around $\delta = \frac{\pi}{2}$. Of course, a full stimulation is needed to confirm this result, which is beyond the scope of this paper.

C. Effect of uncertainties of θ_{23} and θ_{13} on δ

In this subsection, we discuss relative importance between uncertainties of θ_{23} and θ_{13} on δ. Our discussion here will be valid both on and off VOM. As already mentioned, the θ_{23} and the θ_{13} intrinsic degeneracies have many common properties. For example, in near vacuum environment, both the θ_{13} and the θ_{23} intrinsic degeneracies produce $\delta \leftrightarrow \pi - \delta$ ambiguity, and the merging of the true and clone allowed regions around $|\delta| = \frac{\pi}{2}$ results in enhanced errors of δ. Now, one can show, by the similar argument as we have given at the end of Sec. II, that the uncertainties of θ_{13} can affect the sensitivity to δ. Then, the natural question is; Which uncertainties are more important, the one of θ_{13}, or of θ_{23}?

We argue that one can make a rough estimate of the relative importance of θ_{13} and θ_{23} uncertainties on δ determination in the following way. Notice that both of the uncertainties produce shift of the ellipses, up and down, along the diagonal line in the bi-probability plot (see Fig. 1), and this movement results in uncertainty in δ. The uncertainties on θ_{13} and θ_{23}, $\Delta\theta_{13}$ and $\Delta\theta_{23}$, can produce the same amount of shift in the center of ellipse (the first term in the probabilities in (4)) if they satisfy the relationship

$$\Delta\theta_{23}|_{equal} \approx \frac{\Delta\theta_{13}}{\sin\theta_{13}} \tag{13}$$

where we have used the approximation $\sin 2\theta_{23} = 1$. Using the current data of θ_{13}, $\sin^2 2\theta_{23} = 0.089 \pm 0.011$ [1], the uncertainty on θ_{13} is 0.55°, thus using Eq. (13), we can obtain the equivalent shift in θ_{23}, $\Delta\theta_{23}|_{equal} \approx 3.7^\circ$. This is comparable, or smaller than the current uncertainties on θ_{23} given by $0.391 \leq \sin^2\theta_{23} \leq 0.691$ at 90% CL [14], which implies $\Delta\theta_{23}|_{current} \approx 6.7^\circ$ (3.8°) for upward (downward) error at 1σ CL. Therefore, even in the current situation the uncertainty of θ_{23} can be larger by a factor of $\simeq 2$ than that due to the θ_{13} error. Since the error of θ_{13} is expected to become much smaller by the continuing θ_{13} measurements at the time when measurement of δ is performed, reducing the θ_{23} error is of crucial importance for an accurate measurement of δ.

IV. SIMULTANEOUS MEASUREMENT OF θ_{23} AND δ: GENERAL CASE

In this section we present solutions of s_{23}^2 and δ for a given set of measurement of P and $\bar{P}$ at generic value of Δ. Instead of giving the explicit solutions we describe an iterative

procedure to obtain the solutions of the degeneracy equations. The explicit solutions of the degeneracy equations are given in Appendix C.

A. Properties of the intrinsic $\theta_{23} - \delta$ degeneracy

To display characteristic properties of the intrinsic $\theta_{23} - \delta$ degeneracy we derive approximate relationship between the degenerate solutions. We define differences between two degenerate solutions as $\Delta s^2_{23} \equiv (s^2_{23})_1 - (s^2_{23})_2$, $\Delta(\sin\delta) \equiv \sin\delta_1 - \sin\delta_2$, and $\Delta(\cos\delta) \equiv \cos\delta_1 - \cos\delta_2$. Using (4) we obtain

$$\begin{aligned} \Delta(\cos\delta)\cos\Delta &= -\frac{(\bar{A}_\oplus + A_\oplus)}{2\ (\epsilon A_\odot)}\ \frac{\Delta s^2_{23}}{\sin 2\theta_{23}}, \\ \Delta(\sin\delta)\sin\Delta &= -\frac{(\bar{A}_\oplus - A_\oplus)}{2\ (\epsilon A_\odot)}\ \frac{\Delta s^2_{23}}{\sin 2\theta_{23}}, \end{aligned} \tag{14}$$

under the approximation that $\sin 2\theta_{23}$ for the two solution is nearly equal, which is in fact an excellent approximation. This feature allows us to derive a simple relation for $\Delta(\sin\delta)$ as in (14), which is different from the θ_{13} intrinsic degeneracy.

From (14) one can infer two important characteristic properties of the $\theta_{23} - \delta$ degeneracy.

- The difference in $\sin\delta$ comes from the matter effect, and hence $\Delta(\sin\delta)$ has to vanish in vacuum and the two solutions exhibit the $\delta \leftrightarrow \pi - \delta$ degeneracy.
- At any VOM, ($\cos\Delta = 0$), Δs^2_{23} has to vanish. It is because the ellipses have zero width at VOM and again the two solutions exhibit the $\delta \leftrightarrow \pi - \delta$ degeneracy.

Therefore, a measurement near VOM can primarily determine only $\sin\delta$, and in that case $\delta \leftrightarrow \pi - \delta$ degeneracy remains. Spectral information around VOM, if available, can be used to break this degeneracy.

B. Solution to the $\theta_{23} - \delta$ degeneracy equation

We start from (8) and (9) which we call the zeroth-order solutions. Notice that we keep value of Δ in $A_\oplus$ and $\bar{A}_\oplus$ generic here, though it has been set to $\frac{\pi}{2}$ when we have discussed the solutions at VOM in the previous section. Under this understanding, we denote the zeroth-order solutions in (8) and (9) as $(s^2_{23})_0$ and δ_0, respectively, in this section. By going back to the original equations (4) and using the zeroth-order solutions (8) and (9) one can derive the equations

$$s^2_{23} = (s^2_{23})_0 - \sin 2\theta_{23} \frac{2\epsilon A_\odot}{\left(A_\oplus + \bar{A}_\oplus\right)} \cos\Delta\cos\delta \tag{15}$$

$$\left(\bar{A}_\oplus + A_\oplus\right)\sin\Delta\sin\delta - \left(\bar{A}_\oplus - A_\oplus\right)\cos\Delta\cos\delta = \left(\bar{A}_\oplus + A_\oplus\right)\sin\delta_0 \tag{16}$$

which can be solved iteratively[4] to find the solution at generic values of Δ.

[4] Start with $s^2_{23} = 1/2$ and calculate $\sin\delta_0$ using Eq. (9). Obtain δ from the solutions of Eq. (16) and then use Eq. (15) to obtain s^2_{23} and iterate. Since $\sin\delta_0$ depends on $\sin 2\theta_{23}$, the change in δ will be small and the iteration will converge rapidly near maximal mixing.

The second equation in (16) can be solved to produce the two solutions

$$\begin{aligned}
\delta &= \phi + \arcsin\left(\frac{\left(\bar{A}_\oplus + A_\oplus\right)\sin\delta_0}{\sqrt{\bar{A}_\oplus^2 + A_\oplus^2 - 2\bar{A}_\oplus A_\oplus \cos 2\Delta}}\right), \\
\delta &= \phi + \pi - \arcsin\left(\frac{\left(\bar{A}_\oplus + A_\oplus\right)\sin\delta_0}{\sqrt{\bar{A}_\oplus^2 + A_\oplus^2 - 2\bar{A}_\oplus A_\oplus \cos 2\Delta}}\right)
\end{aligned} \tag{17}$$

where

$$\begin{aligned}
\cos\phi &\equiv \frac{\left(\bar{A}_\oplus + A_\oplus\right)\sin\Delta}{\sqrt{\bar{A}_\oplus^2 + A_\oplus^2 - 2\bar{A}_\oplus A_\oplus \cos 2\Delta}}, \\
\sin\phi &\equiv \frac{\left(\bar{A}_\oplus - A_\oplus\right)\cos\Delta}{\sqrt{\bar{A}_\oplus^2 + A_\oplus^2 - 2\bar{A}_\oplus A_\oplus \cos 2\Delta}}.
\end{aligned} \tag{18}$$

Note, at VOM $\phi = 0$ and thus the two solutions exhibit the $\delta \leftrightarrow \pi - \delta$ degeneracy and they have the same value of s_{23}^2 since $\cos\Delta = 0$. In vacuum, Eq. (16) reduces to $\sin\delta = \sin\delta_0/\sin\Delta$, so that $\sin\delta$ is determined but $\cos\delta$ has two signs so that different values of s_{23}^2 are possible, provided that we are not at VOM.

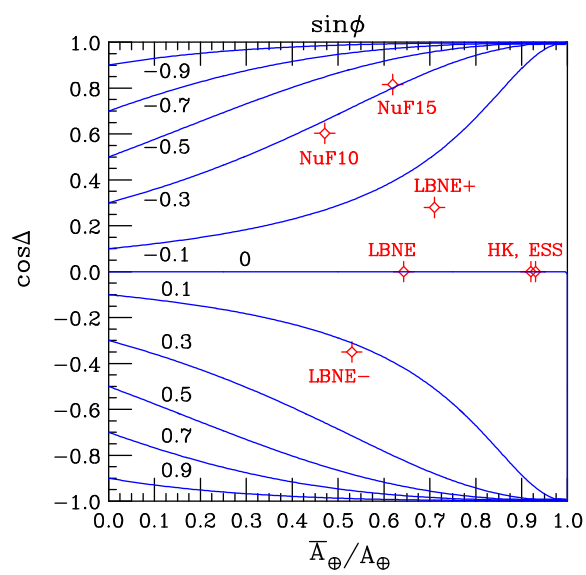

FIG. 2: Equi-$\sin\phi$ contours are plotted on $\frac{\bar{A}_\oplus}{A_\oplus}$ vs. $\cos\Delta$ plane assuming the normal mass hierarchy. The typical values of $\frac{\bar{A}_\oplus}{A_\oplus}$ and $\cos\Delta$ to be examined in Sec. V are also shown by asterisks; LBNE$\pm$ denote the cases with 20% higher (+) and lower (−) energies than the one of the LBNE setting at VOM, and NuF10 and NuF15 stand for neutrino factory setting with energy 10 GeV and 15 GeV, respectively.

We plot in Fig. 2 the contours of equal $\sin\phi$ line on $\frac{\bar{A}_\oplus}{A_\oplus}$ vs. $\frac{\Delta}{\pi}$ plane, assuming the normal mass hierarchy for which $0 \leq \frac{\bar{A}_\oplus}{A_\oplus} \leq 1$. For the inverted mass hierarchy the abscissa must be

interpreted as $\frac{A_\oplus}{\bar{A}_\oplus}$.[5] In Fig. 2 we also show by asterisks the points to be examined in Sec. V with typical values of the various settings of experiments proposed. It is remarkable to see that in all cases $\sin\phi$ is small, despite one's naive expectation that might expect become large when matter effects are large e.g., in the LBNE and neutrino factory settings.

V. FEATURES OF SIMULTANEOUS MEASUREMENT OF θ_{23} AND δ IN SOME EXPERIMENTAL SETTINGS

In this section, we examine features of simultaneous measurement of θ_{23} and δ by considering several experimental settings with their typical parameters (baseline and energy). In the course of analysis, we illuminate some characteristic features of the θ_{23} intrinsic degeneracy. Though our analysis is based on assumed measurement of oscillation probabilities P and $\bar{P}$ with errors, it may capture main features of the more extensive analysis with cross sections, efficiencies, energy spectra etc. with systematic errors. We hope to come back to such an analysis in the future. We start by describing our analysis method.

A. Analysis method

We define the model χ^2 which is used in our analysis as follows:

$$\chi^2(\theta_{23},\delta) = \frac{(P(\theta_{23},\delta) - P(\theta_{23}^x,\delta^x))^2}{(\Delta P)^2} + \frac{(\bar{P}(\theta_{23},\delta) - \bar{P}(\theta_{23}^x,\delta^x))^2}{(\Delta \bar{P})^2} \tag{19}$$

where θ_{23}^x and δ^x are the test values for θ_{23} and δ. In our analysis χ^2 is computed only at some fixed values of neutrino energy and spectrum information is not taken into account.

We determine the errors to be placed on measurement of P and $\bar{P}$ in the following way. The number of event N in a single "energy bin" may be calculated as $N = n_T \int dE f(E) \frac{d\sigma}{dE} P \approx n_T f_0 \frac{d\sigma}{dE} P$, where n_T denotes target number density and $f_0 = f(E)\Delta E$ is the neutrino flux in a particular energy bin of width ΔE. Ignoring the systematic uncertainties on flux, cross sections, and target number density, and assuming the remaining uncertainties are of statistical nature only, then $\frac{\Delta N}{N} = \frac{\Delta P}{P} \propto 1/\sqrt{P}$ since ΔN varies as $\sqrt{N}$. Thus, we will assume the fractional uncertainty on the oscillation probabilities are given by

$$\frac{\Delta P}{P} = 0.03\sqrt{\frac{P_0}{P}}, \qquad \frac{\Delta \bar{P}}{\bar{P}} = 0.03\sqrt{\frac{\bar{P}_0}{\bar{P}}}. \tag{20}$$

The reference probabilities are taken as $P_0 = \bar{P}_0 = \sin^2\theta_{23}\sin^2 2\theta_{13} = 0.5 \times 0.09 = 0.045$, so that about 1100 events are assumed at the reference point, Equation (20) will be referred to as "3% error" throughout this section. (In Sec. V C, we will use 1% error just by replacing 0.03 by 0.01 in (20) in a neutrino factory analysis.)

[5] In a very limited phase space $\frac{\bar{A}_\oplus}{A_\oplus}$ can be negative. But since it does not occur in most of the proposed settings we do not enter into this possibility here.

B. Hyper-K vs. LBNE

Let us start by examining the Hyper-K and the LBNE settings at the VOM, by which we mean $E = 0.6$ GeV and $L = 295$ km for Hyper-K [13], and $E = 2.6$ GeV and $L = 1300$ km for the LBNE settings [15], respectively. In Fig. 3, the allowed contours at 1σ, 2σ, and 3σ CL (2 d.o.f.) in δ/π vs. $\sin^2\theta_{23}$ space are presented in which a 3% error is assumed for both P and $\bar{P}$ measurement. Three sets of values of δ and $\sin^2\theta_{23}$ are used as inputs: (0°, 0.5) shown by black contour, (45°, 0.45) by blue contours, and (−60° 0.55) by red contours. They are shown by + symbol in the figure, the style we keep throughout this section.

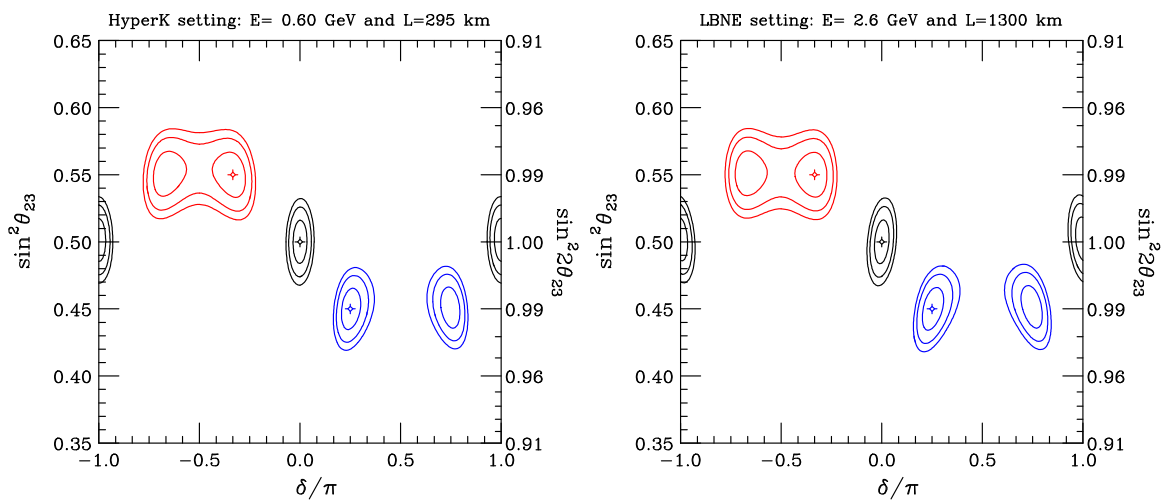

FIG. 3: Contours of allowed regions at 1σ, 2σ, and 3σ CL (2 d.o.f.) in δ/π vs. $\sin^2\theta_{23}$ space assuming 3% error for both P and $\bar{P}$ measurement. The left and right panels are for the Hyper-K and the LBNE settings, respectively. The true values of (δ, $\sin^2\theta_{23}$) are taken as (0°, 0.5) the case shown in black, (45°, 0.45) in blue, and (−60° 0.55) in red.

The features of the allowed regions shown in the left and right panels of Fig. 3 are remarkably similar with each other despite the larger matter effect in the LBNE setting. One may tempted to interpret this feature as simply due to that they are both at the VOM. But, actually it is not the whole story as explained shortly below.

We observe in Fig. 3 for any one of the inputs two allowed regions corresponding to the true and the clone solutions, a manifestation of the θ_{23} intrinsic degeneracy. They are related by symmetry under $\delta \leftrightarrow \pi - \delta$ as it is clearly visible in the figure. The symmetry reflects the fact that the setting is almost at VOM at which only $\sin\delta$ survives in the oscillation probabilities. It is also notable that true and clone contours are horizontally spaced, $\Delta s_{23}^2 \simeq 0$, the feature which also arises by sitting at VOM, as seen in (14). The allowed regions become larger as $\sin^2\theta_{23}$ get larger because the errors of P and $\bar{P}$ increases by $\approx 10\%$ from $\sin^2\theta_{23} = 0.45$ (blue) to 0.55 (red).

In Fig. 4, the similar contours of allowed regions are plotted with the same Hyper-K and LBNE settings, but with higher (shown in blue) and lower (shown in red) energies by 10% (20%) for Hyper-K (LBNE) than their respective energies at VOM. Our choice of larger variations of energy off VOM reflects the fact that LBNE is equipped with a wide-band neutrino beam. In fact, if we choose the same rate of variation of energy for Hyper-K and

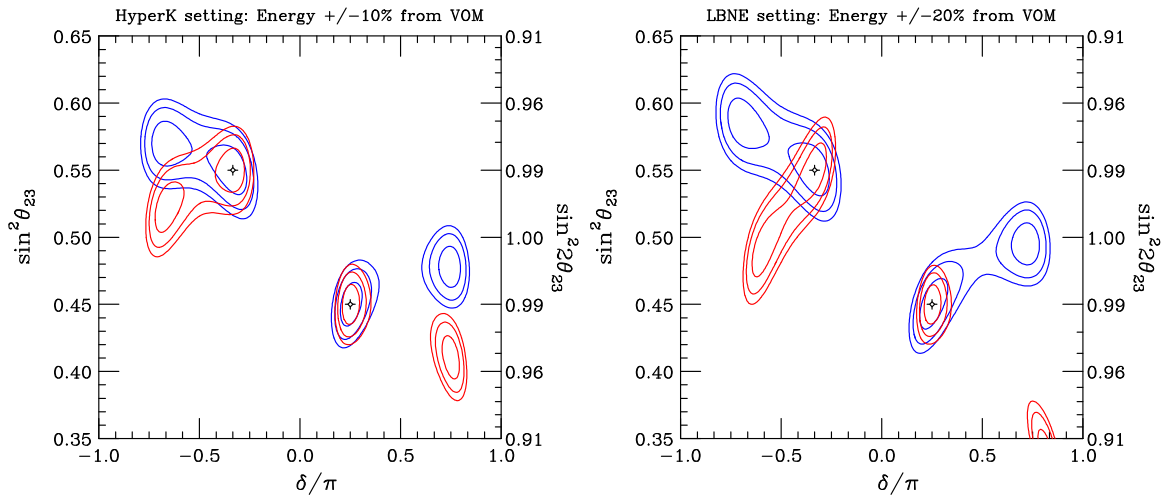

FIG. 4: The same as in Fig. 3 but with higher ($\Delta < \frac{\pi}{2}$, shown in blue) or lower ($\Delta > \frac{\pi}{2}$, shown in red) neutrino energies by ±10% (Hyper-K) and ±20% (LBNE) than the ones of VOM. The true values of (δ, $\sin^2\theta_{23}$) are taken as (45°, 0.45) shown in blue, and (−60° 0.55) shown in red.

LBNE the features of the contours are almost the same. The matter effect plays little role for this plot. It is because the slope $\frac{\Delta\cos\delta}{\Delta s_{23}^2}$ in (14) is insensitive to the matter effect; it cancels out to leading order in $\frac{a}{\Delta m_{32}^2}$. We observe that the direction of shift of $\cos\delta$ is opposite as that of s_{23}^2 for $\Delta < \frac{\pi}{2}$ (shown in blue), while it goes along the same direction for $\Delta > \frac{\pi}{2}$ (shown in red), as it should be according to (14).

In Fig. 4, we observe that while the allowed regions for the true and the clone solutions remain separated at 1σ CL (apart from the red one with input $s_{23}^2 = 0.55$ for LBNE) they start to merge together at higher CL. Once the merging takes place the errors are governed primarily by distance between the true and the clone solutions, in addition to the uncertainties inherent to the measurement. If this phenomenon occurs in sizable fraction of the parameter space of the analysis the accuracies of measurement of both s_{23}^2 and $\sin\delta$ are significantly lost. To our knowledge, this feature does not appear to be addressed in previously performed sensitivity studies for δ, while it might have been buried into the necessarily intricate simulation procedure.

We notice that the movement of the allowed regions are rather dynamic despite the small shift of the energies in both cases. It suggests that the spectrum informations above and below VOM in the off-axis (narrow band) beam would be important to resolve the θ_{23} intrinsic degeneracy. Naturally, the distances between the degenerate solutions become farther apart for larger energy variation as shown in Fig. 4, suggesting that LBNE with the wide-band beam would be more powerful in resolving the θ_{23} intrinsic degeneracy.

C. A neutrino factory setting

In Fig. 5, the similar allowed contours are presented for a particular setting for neutrino factory [16] with assumed baseline of $L = 3000$ km. Two values of neutrino energy, $E = 10$ GeV and $E = 15$ GeV, are chosen as typical ones which are shown in red and in blue,

respectively. Unlike other cases we take 1% errors for P and $\bar{P}$, which implies $\simeq 10^4$ events in each channel at the reference probabilities $P_0 = \bar{P}_0 = 0.045$. Despite the smaller errors taken discriminating power of the clone solution from the true one is quite limited. Two regions of true and clone solutions merge apart from those in region of $\sin\delta < 0$ at $E = 10$ GeV. Since they are below VOM ($\Delta < \frac{\pi}{2}$) the relationship between true and clone solutions are similar at both energies.

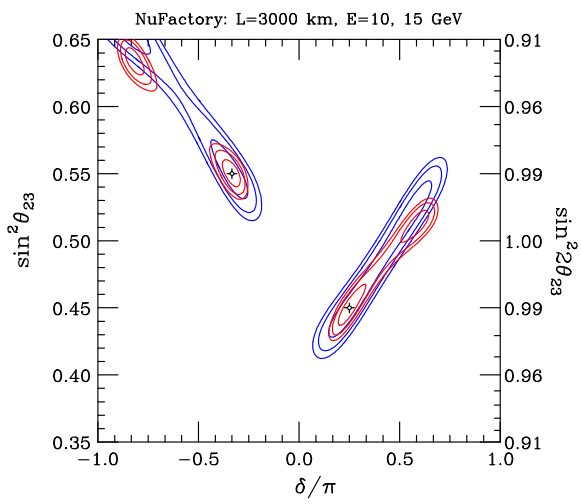

FIG. 5: Contours of allowed regions at 1σ, 2σ, and 3σ CL (2 d.o.f.) in δ/π vs. $\sin^2\theta_{23}$ space for neutrino factory setting with $L = 3000$ km. Two particular values of neutrino energies are taken for comparison, one at $E = 10$ GeV (shown in red) and $E = 15$ GeV (shown in blue). Unlike other cases 1% error is assumed for both P and $\bar{P}$ measurement. The true values of (δ, $\sin^2\theta_{23}$) are taken as (45°, 0.45) and (−60° 0.55).

VI. A SETTING AT THE SECOND OSCILLATION MAXIMUM

In this section we discuss some new aspects that show up when the beam energy is tuned to, or it covers over, the second VOM, $\Delta = \frac{3\pi}{2}$. The most important change in this region is that $A_\odot \propto \Delta$ becomes larger by a factor of three. Then, δ dependent term which comes from interference between $A_\oplus$ and $A_\odot$ gets larger by the same amount. It influences to the errors of s^2_{23} and δ. Δs^2_{23} in (11) remains unchanged if the uncertainties ΔP and $\Delta\bar{P}$ are the same at the 2nd VOM. On the other hand, $\Delta(\sin\delta)$ becomes smaller by a factor of three, implying a better sensitivity to CP at the 2nd VOM. Therefore, Eq. (12) is modified to $\Delta(s^2_{23}) \simeq \frac{1}{2}\Delta(\sin\delta)$.

To elucidate the new features of the setting at 2nd VOM we examine the case with ESS (European Spallation Source) [17], the facility to be build in Sweden which plans to produce 5 MW of beam power which can be used to construct intense neutrino beam. The baseline to a detector is assumed to be $L = 540$ km and the energy at around the 2nd VOM is given approximately as $E = 0.353$ GeV. In Fig. 6 presented are the contours of allowed regions by assuming 3% measurement of P and $\bar{P}$. We take neutrino energies 3% higher (0.364 GeV, $\Delta < \frac{\pi}{2}$, shown in blue), or 3% lower (0.342 GeV, $\Delta > \frac{\pi}{2}$, shown in red) than that of 2nd VOM.

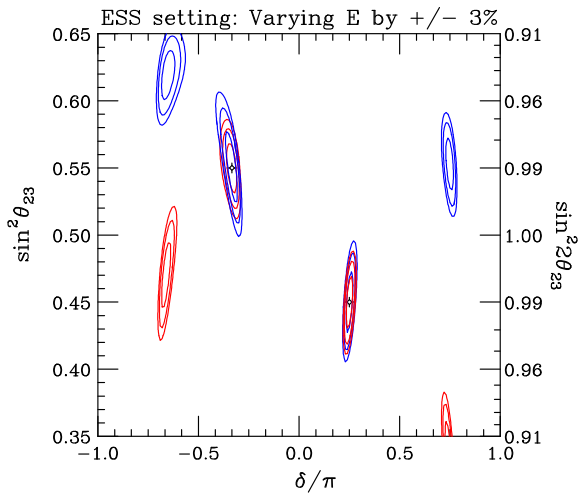

FIG. 6: Contours of allowed regions at 1σ, 2σ, and 3σ CL (2 d.o.f.) in δ/π vs. $\sin^2\theta_{23}$ space for ESS setting with $L = 540$ km. Two particular values of neutrino energies are taken for comparison, one at $E = 0.342$ GeV (shown in red) and $E = 0.364$ GeV (shown in blue), which amount to $\pm 3\%$ of the one at 2nd VOM. The true values of (δ, $\sin^2\theta_{23}$) are taken as ($45°$, 0.45) and ($-60°$ 0.55).

One notices that the allowed regions significantly shrink along δ direction, the effect we mentioned above. It is also remarkable that clone solutions moves significantly upward or downward despite very small variation of neutrino energy of $\pm$ 3%. It implies that resolving power of the θ_{23} intrinsic degeneracy, in principle, can be higher at the 2nd VOM.

VII. CONCLUSION

In this paper, we have shown that s^2_{23} can be determined automatically at higher accuracies than $\sin\delta$ in experiments which can measure δ using ν_e and $\bar{\nu}_e$ appearance channels. The accuracy for s^2_{23} determination supersedes that of the conventional method which relies on ν_μ disappearance channels in region $40° \lesssim \theta_{23} \lesssim 50°$, assuming high enough statistics that allows reasonable precision on the measurement of CP phase, δ. The reasons for such high accuracy is that the appearance method is free from the problems of Jacobian broadening in the translation $\sin^2 2\theta_{23} \to s^2_{23}$ for values of θ_{23} near $45°$, and of the determination of the octant of θ_{23}.

With use of ν_e and $\bar{\nu}_e$ appearance channels, determination of θ_{23} is inherently coupled with measurement of CP phase δ. Thus, the uncertainties on the measurement of θ_{23} and δ are correlated. Furthermore, our treatment reveals that measurement of the two independent parameters metamorphoses into a new strategy which may be called as "simultaneous measurement of θ_{23} and δ". Reflecting on the nature of these measurements, a new parameter degeneracy called the "θ_{23} intrinsic degeneracy" is identified. In general, two degenerate solutions of θ_{23} and δ are given for each set of measurements of oscillation probabilities, P and $\bar{P}$, producing a new ambiguity and a new source of uncertainties, hitherto unrecognized. This degeneracy must be resolved to make an accurate determination of both θ_{23} and δ.

To understand characteristic features of correlated measurement of θ_{23} and δ, we have undertaken the following two approaches: (1) Toward resolution of the degeneracy, we have

analyzed the natures of the θ_{23} intrinsic degeneracy, and obtained the analytic formulas for the degeneracy solutions which help us to understand characteristic features of the degeneracy. (2) We have simulated simple data set of P and $\bar{P}$ with suitably assumed errors to obtain the contours of allowed regions in s_{23}^2 vs. δ space. We have examined various settings, Hyper-K, LBNE, and neutrino factory all around (or below) 1st VOM, and ESS (European Spallation Source) near 2nd VOM, using their typical values of baseline and neutrino energies.

From these studies we have observed the following features of our new method, simultaneous measurement of θ_{23} and δ. The obtained contours of allowed regions confirm our expectation that the error of s_{23}^2 determination is approximately six times smaller than that of $\sin\delta$ apart from the problem of merging the degeneracy solutions. Importantly, the movement of clone solutions against varying energy is generally quite large, and the effect is more significant around 2nd VOM than the 1st VOM. Thus, we have uncovered the crucial point that spectrum information is of key importance to resolve the θ_{23} intrinsic degeneracy. This feature is reminiscent of the one encountered in the θ_{13} intrinsic degeneracy.

In addition, the contours of allowed regions revealed some characteristic features of the θ_{23} intrinsic degeneracy, such as $\delta \to \pi - \delta$ symmetry, in most of the settings we discussed. While the feature must hold at VOM or in vacuum, its robustness in fact requires explanation. We have shown that it can be understood by our analytical expressions of the degeneracy solutions, which implies that the matter effect plays only a minor role in the relationship between the two solutions of δ.

We have concluded that our new method, using ν_e appearance channels, offers a better way of measuring θ_{23} with high accuracy, in the region $40^\circ \lesssim \theta_{23} \lesssim 50^\circ$ in particular, and the simultaneous measurement of θ_{23} and δ is the right strategy to carry out precision measurement of the both parameters. Incorporation of these ideas into a full stimulation will be undertaken in a follow up paper [18].

Appendix A: Uncertainty of δ from Probabilities and s^2_{23}

In this Appendix, we calculate the uncertainties in $\cos\delta$ and $\sin\delta$ which would be produced by small measurement uncertainties in P, $\bar{P}$, and s^2_{23}. Here, we do *not* consider s^2_{23} as a parameter determined by our appearance method with $(P, \bar{P})$ measurement, but regard it as an external parameter determined e.g., by using the disappearance channel.

If we start with the appearance probability expressions, Eq. (4), and expand the $\cos(\Delta\pm\delta)$ terms: there are two terms with δ dependence, one proportional to $\sin\delta$ and the other proportional to $\cos\delta$. We then use the chain rule of differentiation, to leading order in $\epsilon \equiv \frac{\Delta m^2_{21}}{\Delta m^2_{31}}$ and for $\cos 2\theta_{23} \ll 1$, to obtain[6]

$$\left.\begin{array}{l}\Delta(\cos\delta\cos\Delta)\\ \Delta(\sin\delta\sin\Delta)\end{array}\right\} = \left(\frac{\tan\theta_{23}}{4}\right)\left[\left(\frac{\bar{A}_\oplus}{\epsilon A_\odot}\right)\frac{\Delta\bar{P}}{\bar{P}} \pm \left(\frac{A_\oplus}{\epsilon A_\odot}\right)\frac{\Delta P}{P} + \left(\frac{\bar{A}_\oplus \pm A_\oplus}{\epsilon A_\odot}\right)\frac{\Delta(s^2_{23})}{s^2_{23}}\right] \quad \text{(A1)}$$

We interpret this result as follows: the uncertainties on the measurement of $(\sin\delta\sin\Delta)$ or of $(\cos\delta\cos\Delta)$, assuming that the uncertainties on P, $\bar{P}$, and s^2_{23} are uncorrelated, are given by

$$\left.\begin{array}{l}\Delta(\cos\delta\cos\Delta)\\ \Delta(\sin\delta\sin\Delta)\end{array}\right\} = \left(\frac{\tan\theta_{23}}{4}\right)\sqrt{\left(\frac{\bar{A}_\oplus}{\epsilon A_\odot}\right)^2(\mathcal{D}\bar{P})^2 + \left(\frac{A_\oplus}{\epsilon A_\odot}\right)^2(\mathcal{D}P)^2 + \left(\frac{\bar{A}_\oplus \pm A_\oplus}{\epsilon A_\odot}\right)^2(\mathcal{D}s^2_{23})^2} \quad \text{(A2)}$$

where $\mathcal{D}O \equiv \frac{\Delta O}{O}$ denotes fractional error of the quantity O.

In vacuum, when $A_\oplus = \bar{A}_\oplus$, it's clear that uncertainty on $\sin\delta$ does not depend on the uncertainty of s^2_{23} whereas the uncertainty on $\cos\delta$ depends strongly on this uncertainty. In matter, however, the uncertainty on both $\sin\delta$ and $\cos\delta$ will depend on the uncertainty on s^2_{23}. One needs both measurements to make a precise measurement of δ otherwise the measurement will suffer from a degeneracy similar to the $\delta \leftrightarrow \pi - \delta$ degeneracy seen at VOM. In the Introduction we simplified this rather complicate situation to make a point regarding the importance of an accurate determination of s^2_{23}.

In near vacuum environment, $\frac{a}{\Delta m^2_{31}} \ll 1$, $\bar{A}_\oplus \approx A_\oplus$ and we have $\frac{\tan\theta_{23}}{4}\frac{A_\oplus}{\epsilon A_\odot} \simeq \frac{6}{4} \simeq 1.5$, which entails the coefficients in $\sqrt{\sum_X(\delta X)^2}$ in (A2) of order unity. Therefore, in near vacuum, an estimation of the uncertainties on $(\sin\delta\sin\Delta)$ (or $(\cos\delta\cos\Delta)$) are given by a very simple expressions

$$\text{Uncertainty of } (\sin\delta\sin\Delta) \sim f_{\text{error}}\sqrt{(\mathcal{D}P)^2 + (\mathcal{D}\bar{P})^2}, \quad \text{(A3)}$$

$$\text{Uncertainty of } (\cos\delta\cos\Delta) \sim f_{\text{error}}\sqrt{(\mathcal{D}P)^2 + (\mathcal{D}\bar{P})^2 + 4(\mathcal{D}s^2_{23})^2} \quad \text{(A4)}$$

where f_{error} is a coefficient of order unity.[7] Thus, for $|\sin\delta|$ near 1, where a precise measurement of $\cos\delta$ is important for an accurate determination of the angle δ, the uncertainty in

[6] Eqs. (A1) and (A2) is more accurate if you interpret P and $\bar{P}$ in the denominator in the first two terms of these equations as $\langle P\rangle$ and $\langle\bar{P}\rangle$, the ones averaged over δ. In other words $\langle P\rangle$ and $\langle\bar{P}\rangle$ imply the coordinate of the center of the bi-P ellipses.

[7] In matter there exists $\eta(\mathcal{D}s^2_{23})^2$ term in the square root in (A3) but with small coefficient. For example, $\eta \simeq 0.24$ for LBNE.

s_{23}^2 plays a significant role. The feature that $\sin\delta$ does not depend on s_{23}^2 while $\cos\delta$ does in the near vacuum environment can be easily understood by the bi-probability plot given in the right panel of Fig. 1. When s_{23}^2 is varied within the uncertainty "center of gravity" of the ellipse moves along the diagonal line in $P-\bar{P}$ plane, which affects predominantly $\cos\delta$ but not so much to $\sin\delta$, as this is a measure of the distance away from the diagonal.

The results in (A3) and (A4) are consistent with each other because here $\sin\delta$ and $\cos\delta$ are treated as independent. Otherwise, the relationship $\Delta(\cos\delta) = -\tan\delta\Delta(\sin\delta)$ must hold.

Appendix B: Errors of s_{23}^2 and δ off the VOM

One may ask the question; Can one derive the formula of errors of s_{23}^2 and δ analogous to (11) in general setting off VOM and without vacuum dominated approximation? In this Appendix we give an answer to this question.

We start from the expressions of P and $\bar{P}$ in (4). We denote the changes of P and $\bar{P}$ induced by a small changes of s_{23}^2 and δ as ΔP and $\Delta\bar{P}$. Conversely, it may interpreted as the relations between small shifts of s_{23}^2 and δ and their cause, i.e., errors of P and $\bar{P}$. To leading order in the small variations we obtain the relationship between the shifts Δs_{23}^2, $\Delta\delta$, ΔP and $\Delta\bar{P}$ as

$$\Delta s_{23}^2 \approx \frac{\left[\Delta\bar{P}\ \left(\frac{A_\oplus}{\bar{A}_\oplus}\right)^{\frac{1}{2}}\sin(\Delta+\delta) + \Delta P\ \left(\frac{\bar{A}_\oplus}{A_\oplus}\right)^{\frac{1}{2}}\sin(\Delta-\delta)\right]}{2\sqrt{\bar{A}_\oplus A_\oplus}\left[\left(\bar{A}_\oplus + A_\oplus\right)\sin\Delta\cos\delta + \left(\bar{A}_\oplus - A_\oplus\right)\cos\Delta\sin\delta\right]}, \tag{B1}$$

$$\Delta\delta \approx \frac{\left[\Delta\bar{P}\ \left(\frac{A_\oplus}{\bar{A}_\oplus}\right) - \Delta P\ \left(\frac{\bar{A}_\oplus}{A_\oplus}\right)\right]}{2\sin 2\theta_{23}(\epsilon A_\odot)\left[\left(\bar{A}_\oplus + A_\oplus\right)\sin\Delta\cos\delta + \left(\bar{A}_\oplus - A_\oplus\right)\cos\Delta\sin\delta\right]}, \tag{B2}$$

where we have ignored the variation of $\sin 2\theta_{23}$ to derive these expressions, since we are only interested in the region near maximal mixing.

From these expressions it is straightforward to derive the formulas of errors of s_{23}^2 and δ by assuming that the errors of P and $\bar{P}$ are independent with each other, and by ignoring errors in neutrino energies, Δm_{32}^2, and etc. They generalize (11) to the case in matter and off VOM. Notice that these expressions of errors are obtained in our appearance method for simultaneous measurement of θ_{23} and δ, and they should not be confused with the errors discussed in Appendix A.

Appendix C: Solution of the Degeneracy Equation

Here, we obtain explicit solutions to the degeneracy problem involving s_{23} and δ.

1. General solutions within the normal hierarchy

By using (4) we obtain

$$\begin{aligned}
\cos\Delta\cos\delta &= \frac{1}{4\epsilon\sin 2\theta_{23}A_\odot}\left[\left(\frac{\bar{P}}{\bar{A}_\oplus}+\frac{P}{A_\oplus}\right)-2s_{23}^2\left(\bar{A}_\oplus+A_\oplus\right)\right],\\
\sin\Delta\sin\delta &= \frac{1}{4\epsilon\sin 2\theta_{23}A_\odot}\left[\left(\frac{\bar{P}}{\bar{A}_\oplus}-\frac{P}{A_\oplus}\right)-2s_{23}^2\left(\bar{A}_\oplus-A_\oplus\right)\right].
\end{aligned} \tag{C1}$$

Then, the equality $\cos^2\delta+\sin^2\delta=1$ can be written in a form of quadratic equation for $x\equiv s_{23}^2$:

$$ax^2-bx+c=0 \tag{C2}$$

where

$$\begin{aligned}
a &= \left(\bar{A}_\oplus^2+A_\oplus^2\right)-2\bar{A}_\oplus A_\oplus\cos 2\Delta+4\epsilon^2A_\odot^2\sin^2 2\Delta\\
b &= \left(\bar{P}+P\right)-\left(\frac{\bar{P}}{\bar{A}_\oplus}A_\oplus+\frac{P}{A_\oplus}\bar{A}_\oplus\right)\cos 2\Delta+4\epsilon^2A_\odot^2\sin^2 2\Delta\\
c &= \frac{1}{4}\left[\left(\frac{\bar{P}}{\bar{A}_\oplus}\right)^2+\left(\frac{P}{A_\oplus}\right)^2-2\left(\frac{\bar{P}}{\bar{A}_\oplus}\right)\left(\frac{P}{A_\oplus}\right)\cos 2\Delta\right]
\end{aligned} \tag{C3}$$

The solution to (C2) is of course given by

$$x=\frac{b\pm\sqrt{b^2-4ac}}{2a} \tag{C4}$$

The solutions for $\cos\delta$ and $\sin\delta$ can be obtained by inserting (C4) into (C1). The discriminant $D\equiv b^2-4ac$ is given by

$$\begin{aligned}
D &= \sin^2 2\Delta\Bigg[-\left(\frac{\bar{P}}{\bar{A}_\oplus}A_\oplus-\frac{P}{A_\oplus}\bar{A}_\oplus\right)^2\\
&+ 4\epsilon^2A_\odot^2\left\{2(\bar{P}+P)-\left(\frac{\bar{P}}{\bar{A}_\oplus}^2+\frac{P}{A_\oplus}^2\right)-2\cos 2\Delta\left(\frac{\bar{P}}{\bar{A}_\oplus}A_\oplus+\frac{P}{A_\oplus}\bar{A}_\oplus-\frac{\bar{P}}{\bar{A}_\oplus}\frac{P}{A_\oplus}\right)\right\}\\
&+ 16\epsilon^4A_\odot^4\sin^2 2\Delta\Bigg]
\end{aligned} \tag{C5}$$

When $D>0$ (C4) describes two solutions of s_{23} and δ for a given set of observable P and $\bar{P}$. By inserting them into (C1) one obtains the corresponding solutions of $\cos\delta$ and $\sin\delta$.

The degeneracy solutions within the alternative (flipped Δ-sign) mass hierarchy can be obtained by making replacements $\Delta\to-\Delta$, $A_\oplus\to-\bar{A}_\oplus$, and $\bar{A}_\oplus\to-A_\oplus$ in (C4) and (C3).

2. Perturbation around the zeroth-order solution

We obtain perturbative solution of $s_{23}^2\equiv x$ and δ in a form $x=x_0+x_1$, and $\delta=\delta_0+\delta_1$ to leading order of small deviation of $\Delta=\frac{\pi}{2}-y$. Here, x_0 and δ_0 imply the zeroth-order

solution given in (8) and (9).[8] Notice that $\cos\Delta \approx y$, $\cos 2\Delta \approx -1 + \frac{y^2}{2}$, and $\sin 2\Delta \approx 2y$. We obtain the equation for x_1:

$$\begin{aligned} &\left(\bar{A}_\oplus + A_\oplus\right)^2 x_1^2 \\ &= 4\epsilon^2 A_\odot^2 \sin 2\theta_{23} y^2 + 4\bar{A}_\oplus A_\oplus x_0^2 y^2 - 2\left(\frac{\bar{P}}{\bar{A}_\oplus} A_\oplus + \frac{P}{A_\oplus}\bar{A}_\oplus\right) x_0 y^2 + \frac{\bar{P}}{\bar{A}_\oplus}\frac{P}{A_\oplus} y^2 \end{aligned} \tag{C6}$$

where a small changes to $\sin 2\theta_{23}$ due to correction to x_0 is ignored. The solution to this equation is given by

$$x_1 = \pm \frac{y}{\left(\bar{A}_\oplus + A_\oplus\right)} 2\epsilon A_\odot \sin 2\theta_{23} \cos\delta_0 \tag{C7}$$

where we have used (9). Using $\sin(\delta_0 + \delta_1) \approx \sin\delta_0 + \delta_1 \cos\delta_0$ in (C1) one obtains, ignoring order y^2 term,

$$\delta_1 \;=\; -\frac{\bar{A}_\oplus - A_\oplus}{2\epsilon A_\odot \sin 2\theta_{23}} x_1 = \mp y \frac{\bar{A}_\oplus - A_\oplus}{\bar{A}_\oplus + A_\oplus} \cos\delta_0 \tag{C8}$$

where we have used (C7). The correction to δ comes from the matter effect, whereas the one to $x = s_{23}^2$ is dominantly vacuum effect.

Acknowledgments

We thank Pilar Coloma for useful discussions. H.M. thanks Theory Group of Fermilab for warm hospitality during visit in winter in 2012-2013 where this work was started and essentially completed. He is grateful to CNPq for support which enables him to visit to Dept. Física, PUC in Rio de Janeiro. He is also supported in part by KAKENHI received through TMU, Grant-in-Aid for Scientific Research No. 23540315, Japan Society for the Promotion of Science.

S.P. acknowledges partial support from the European Union FP7 ITN INVISIBLES (Marie Curie Actions, PITN- GA-2011- 289442). Fermilab is operated by the Fermi Research Alliance under contract no. DE-AC02-07CH11359 with the U.S. Department of Energy.

[1] F. P. An *et al.* [DAYA-BAY Collaboration], Phys. Rev. Lett. **108**, 171803 (2012) [arXiv:1203.1669 [hep-ex]]; arXiv:1210.6327 [hep-ex].

[2] J. K. Ahn *et al.* [RENO Collaboration], Phys. Rev. Lett. **108**, 191802 (2012) [arXiv:1204.0626 [hep-ex]].

[8] Strictly speaking, since we do not take $\Delta = \frac{\pi}{2}$ in $A_\odot$ and $\bar{A}_\odot$ in zeroth-order solutions it is not quite the perturbative expansion. Yet, it is a useful way to obtain approximate solutions near the VOM. It may be justified when $\bar{A}_\oplus$ and $A_\oplus$ are slowly varying around VOM. When we really talk about the solution at VOM, $A_\odot$ and $\bar{A}_\odot$ must be interpreted as taking $\Delta = \frac{\pi}{2}$ in them.

[3] Y. Abe *et al.* [DOUBLE-CHOOZ Collaboration], Phys. Rev. Lett. **108**, 131801 (2012) [arXiv:1112.6353 [hep-ex]]; Phys. Rev. D **86**, 052008 (2012) [arXiv:1207.6632 [hep-ex]].
[4] K. Abe *et al.* [T2K Collaboration], Phys. Rev. Lett. **107**, 041801 (2011) [arXiv:1106.2822 [hep-ex]].
[5] P. Adamson *et al.* [MINOS Collaboration], Phys. Rev. Lett. **107**, 181802 (2011) [arXiv:1108.0015 [hep-ex]]; [arXiv:1301.4581 [hep-ex]].
[6] R. Wendell *et al.* [Super-Kamiokande Collaboration], Phys. Rev. D **81**, 092004 (2010) [arXiv:1002.3471 [hep-ex]].
[7] P. Adamson *et al.* [MINOS Collaboration], Phys. Rev. Lett. **106**, 181801 (2011) [arXiv:1103.0340 [hep-ex]].
[8] H. Minakata, M. Sonoyama and H. Sugiyama, Phys. Rev. D **70**, 113012 (2004) [hep-ph/0406073].
[9] J. Burguet-Castell, M. B. Gavela, J. J. Gomez-Cadenas, P. Hernandez and O. Mena, Nucl. Phys. B **608**, 301 (2001) [hep-ph/0103258].
[10] G. L. Fogli and E. Lisi, Phys. Rev. D **54**, 3667 (1996) [arXiv:hep-ph/9604415].
[11] H. Minakata and H. Nunokawa, JHEP **0110**, 001 (2001) [arXiv:hep-ph/0108085].
[12] P. Coloma, A. Donini, E. Fernandez-Martinez and P. Hernandez, JHEP **1206**, 073 (2012) [arXiv:1203.5651 [hep-ph]].
[13] K. Abe, *et al.*, "Letter of Intent: The Hyper-Kamiokande Experiment — Detector Design and Physics Potential —," arXiv:1109.3262 [hep-ex].
[14] Y. Itow, Talk at XXIV International Conference on Neutrino Physics and Astrophysics (Neutrino 2012), Kyoto, Japan, June 3-9, 2012.
[15] T. Akiri *et al.* [LBNE Collaboration], arXiv:1110.6249 [hep-ex].
[16] A. Bandyopadhyay *et al.* [ISS Physics Working Group Collaboration], Rept. Prog. Phys. **72**, 106201 (2009) [arXiv:0710.4947 [hep-ph]].
[17] E. Baussan, M. Dracos, T. Ekelof, E. F. Martinez, H. Ohman and N. Vassilopoulos, arXiv:1212.5048 [hep-ex].
[18] P. Coloma, H. Minakata, S. Parke, in preparation.